DRAFT VERSION MARCH 26, 2012
Preprint typeset using LaTeX style emulateapj v. 11/26/03

THE EPOCH OF DISK SETTLING: $Z \sim 1$ TO NOW

SUSAN A. KASSIN,[1,2] BENJAMIN J. WEINER,[3] S. M. FABER,[4] JONATHAN P. GARDNER,[1] C. N. A. WILLMER,[3] ALISON L. COIL,[5] MICHAEL C. COOPER,[6,7] JULIEN DEVRIENDT,[8] AARON A. DUTTON,[5] PURAGRA GUHATHAKURTA,[4] DAVID C. KOO,[4] A. J. METEVIER,[9] KAI G. NOESKE,[10] AND JOEL R. PRIMACK[11]

Draft version March 26, 2012

ABSTRACT

We present evidence from a sample of 544 galaxies from the DEEP2 Survey for evolution of the internal kinematics of blue galaxies over $0.2 < z < 1.2$. DEEP2 provides a large sample of high resolution galaxy spectra and dual-band *Hubble* imaging from which we measure emission-line kinematics and galaxy inclinations, respectively. Our large sample allows us to overcome scatter intrinsic to galaxy properties, in order to examine trends. At a fixed stellar mass, galaxies systematically decrease in disturbed motions and increase in rotation velocity and potential well depth with time. The most massive galaxies are the most well-ordered at all times, with higher rotation velocities and less disturbed motions compared to less massive galaxies. We quantify disturbed motions with an integrated gas velocity dispersion (σ_g), which is unlike the typical pressure-supported velocity dispersion measured for early type galaxies and galaxy bulges. Due to finite slit width and seeing, σ_g integrates over unresolved velocity gradients which can correspond to non-ordered gas kinematics such as small-scale velocity gradients, gas motions due to star-formation, or super-imposed clumps along the line-of-sight. We compile surveys of galaxy kinematics over $1.2 < z < 3.8$ and do not find any trends with redshift, likely because these studies are biased toward the most highly star-forming systems. In summary, over the last ~ 8 billion years since $z = 1.2$, blue galaxies evolve from disturbed to ordered systems as they settle to become the rotation-dominated disk galaxies observed in the Universe today, with the most massive galaxies always being the most evolved at any time.

Subject headings: galaxies – formation, galaxies – evolution, galaxies – kinematics and dynamics, galaxies – fundamental properties

1. INTRODUCTION

In the standard picture of disk galaxy formation, baryons enter into dark matter halos and dissipate to form disks at their centers (Rees & Ostriker 1977; White & Rees 1978; Fall & Efstathiou 1980; Blumenthal et al. 1984). The accretion of baryons onto galaxies is expected to be an on-going process, and it is not yet known how galaxy disks respond to it, or how they evolve as mass accretion rates change. Only recently have hydrodynamic simulations begun to address this (Kimm et al. 2011; Danovich et al. 2011). The cleanest observational probe of disk galaxy assembly is internal galaxy kinematics. It tells us directly about the dynamical state of galaxies, reveals the potential well depths of individual galaxy-dark matter halo systems, and can be measured for a large sample of galaxies over a significant range in redshift.

We have acquired a wealth of information about blue galaxies over the last ~ 8 billion years since $z = 1.2$ which can be roughly divided into two categories: those which imply a significant amount of evolution and those which do not. We posit that the best way to resolve these seemingly contradictory results is with a study of the internal kinematics of galaxies. Of those studies which do not imply much evolution are galaxy luminosity functions. They find that the number density of blue galaxies is unchanging, and that blue galaxies fade by only ~ 1 B-band magnitude since $z \sim 1$ (e.g., Willmer et al. 2006; Faber et al. 2007; Bell et al. 2005). Similarly, stellar mass functions of galaxies do not evolve to within uncertainties on the stellar mass measurements (~ 0.2 dex), although there are some hints for a slight decrease in number density with time (Drory et al. 2009). In addition, galaxy sizes are only marginally smaller at $z = 1$ (by a factor of 1.4; Dutton et al. 2011), and the major merger rate of blue galaxies is only $\sim 10 - 20\%$ between $z = 1$ and now (Lotz et al. 2011). However, despite all this evidence for a slowly evolving population, there are some strong indications to the contrary. Namely, blue galaxies at $z \sim 1$ have significantly higher star-formation rates (by a factor of ~ 3; e.g., Noeske et al. 2007), higher molecular gas fractions for at least the brighter galaxies at $z = 1.1 - 1.2$ by a factor of $\sim 2 - 4$** (Daddi et al. 2010; Tacconi et al. 2010), and more disturbed morphologies (e.g., Abraham et al. 1996; Abraham & van den Bergh 2001). In summary, galaxies do not evolve much in luminosity, stellar mass, or size, but they do evolve strongly in star-formation rate, molecular gas mass, and

[1] Astrophysics Science Division, Goddard Space Flight Center, Code 665, Greenbelt, MD 20771, susan.kassin@nasa.gov
[2] NASA Postdoctoral Program Fellow
[3] Steward Observatory, University of Arizona, Tucson, AZ
[4] UCO/Lick Obs., Dept of Astronomy and Astrophysics, University of California, Santa Cruz, CA 95064
[5] Department of Physics, University of California, Santa Barbara, CA 93106
[6] Center for Galaxy Evolution, Department of Physics and Astronomy, University of California, Irvine, 4129 Frederick Reines Hall, Irvine, CA 92697
[7] Hubble Fellow
[8] Department of Physics, Denys Wilkinson Building, Keble Road, Oxford, OX1 3RH, United Kingdom
[9] Department of Physics and Astronomy, Sonoma State University, 1801 E. Cotati Ave., Rohnert Park, CA 94928
[10] Space Telescope Science Institute, 3700 San Martin Drive, Baltimore, MD 21218
[11] Department of Physics, University of California, 1156 High Street, Santa Cruz, CA 95064

morphology. It is unclear what mechanisms are behind these transformations. In this paper, we attempt to understand this discrepancy, and the mechanisms behind it, by studying the internal kinematics of blue galaxies over $0.2 < z < 1.2$.

Due to the large intrinsic scatter in the kinematic properties of blue galaxes (Weiner et al. 2006a,b; Kassin et al. 2007), a sizeable sample ($\gtrsim 100$) which is representative in terms of galaxy properties is required to study internal galaxy kinematics over a significant look-back time. Such a sample is provided by the Deep Extragalactic Evolutionary Probe 2 Survey (DEEP2; Newman et al. 2012). DEEP2 is one of two large galaxy surveys which cover a significant range in redshift and have high enough spectral resolution to measure semi-resolved galaxy kinematics, the other being the much smaller Team Keck Redshift Survey (TKRS; Wirth et al. 2004). These surveys were created with galaxy kinematics in mind. In addition, a portion of DEEP2 galaxies also have *Hubble Space Telescope*/ACS imaging in two bandpasses (V and I; F606W and F814W, respectively). *Hubble* images are required for measurements of galaxy axial ratios, which are needed to correct rotation velocities for inclinations of galaxies to the line-of-sight. The two wavebands allow for axial ratios to be measured at similar rest-frame wavelengths for galaxies over $0.2 < z < 1.2$.

The DEEP2 and TKRS Surveys have revealed that the kinematics of blue galaxies are not fully described by rotation velocity (V_{rot}) alone (Weiner et al. 2006a,b; Kassin et al. 2007). About one-third to one-half of emission-line galaxies over $0.2 < z < 1.2$ have a significant or dominant component of disordered motions, as measured via an integrated gas velocity dispersion (σ_g). The importance of σ_g in galaxy kinematics was also found by surveys using Integral Field Spectroscopy (IFS) of representative galaxies at $z \sim 0.6$ (IMAGES; Yang et al. 2008), and strongly star-forming galaxies at $z \sim 1.3$ (Wright et al. 2007, 2009; Epinat et al. 2009; Lemoine-Busserolle & Lamareille 2010; Vergani et al. 2012), $z \sim 2$ (Förster-Schreiber et al. 2009; Law et al. 2009), and $z \sim 3$ (Lemoine-Busserolle et al. 2010; Gnerucci 2011).

Galaxies with large values of σ_g scatter to low V_{rot} in the Tully-Fisher relation (V_{rot} versus luminosity or stellar mass) (e.g., Kassin et al. 2007). However, when σ_g is incorporated along with V_{rot} into a kinematic indicator which is created to trace the potential wells of galaxy-dark halo systems, namely $S_{0.5} \equiv \sqrt{0.5 V_{rot}^2 + \sigma_g^2}$, a more complete measure of the internal motions of galaxies results. When V_{rot} is replaced by $S_{0.5}$ in the Tully-Fisher relation, there is significantly reduced scatter (Weiner et al. 2006a; Kassin et al. 2007; Catinella et al. 2011). This tightening of Tully-Fisher once $S_{0.5}$ is adopted was also found for IFS observations (Cresci et al. 2009; Puech et al. 2010; Lemoine-Busserolle & Lamareille 2010; Lemoine-Busserolle et al. 2010; Vergani et al. 2012), and numerical simulations of interacting galaxies (Covington et al. 2010). It is clear from these studies that σ_g captures a necessary component of kinematic support, although it is unknown what phenomena cause it. Possibilities include small-scale velocity gradients, gas motions due to star-formation, and super-imposed clumps along the line-of-sight.

Kassin et al. (2007) showed that galaxies evolve in V_{rot} and σ_g since $z = 1.2$, and quantified the evolution in terms of the Tully-Fisher relation. In this paper, we study the evolution of V_{rot}, σ_g and $S_{0.5}$ individually. We ask the following questions of our dataset: Do disks form/settle from an initially disordered state? If so, what are the kinematic signatures of disk settling/formation? Is this process dependent on galaxy properties such as stellar mass and size? What is the fraction of blue galaxies which are settled today and at $z = 1$? A key element of this study is our broad sample selection, which is described in §2. In §3 we discuss the stellar mass and size

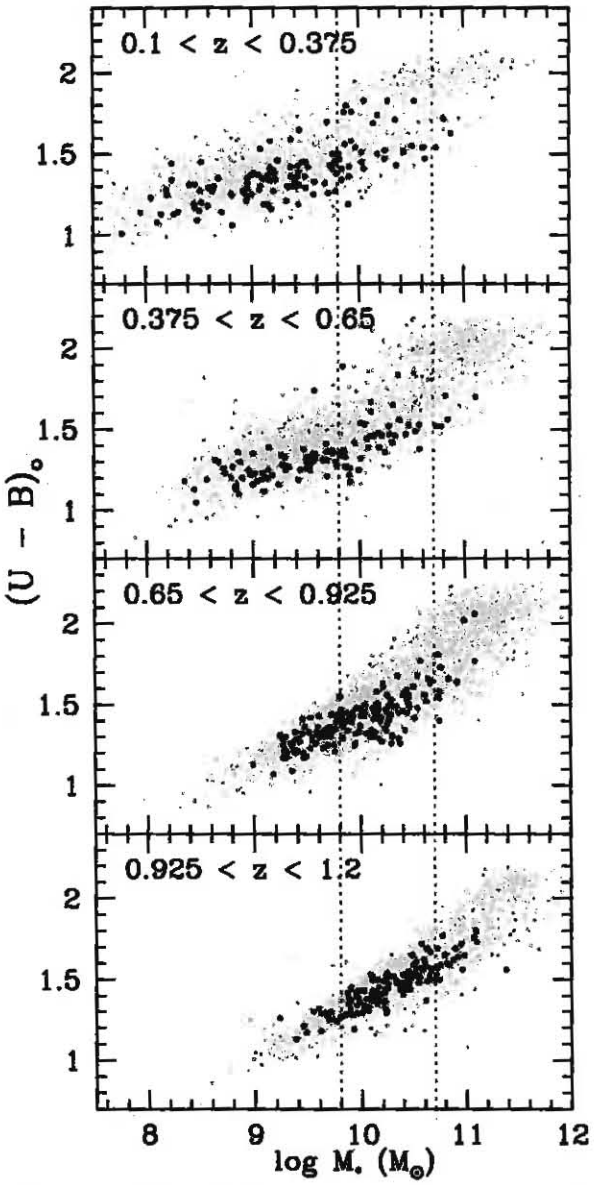

FIG. 1.— Rest-frame $U-B$ color versus stellar mass diagrams for galaxies with solid spectroscopic redshifts in field 1 of the DEEP2 Survey (grey points) and for the K07 sub-sample (black points) are shown in bins of redshift. The K07 sample traces the full stellar mass range of the DEEP2 Survey and a significant range in color in the "blue cloud" at all redshifts. Dotted lines demarcate the mass-complete sample used later in this paper.

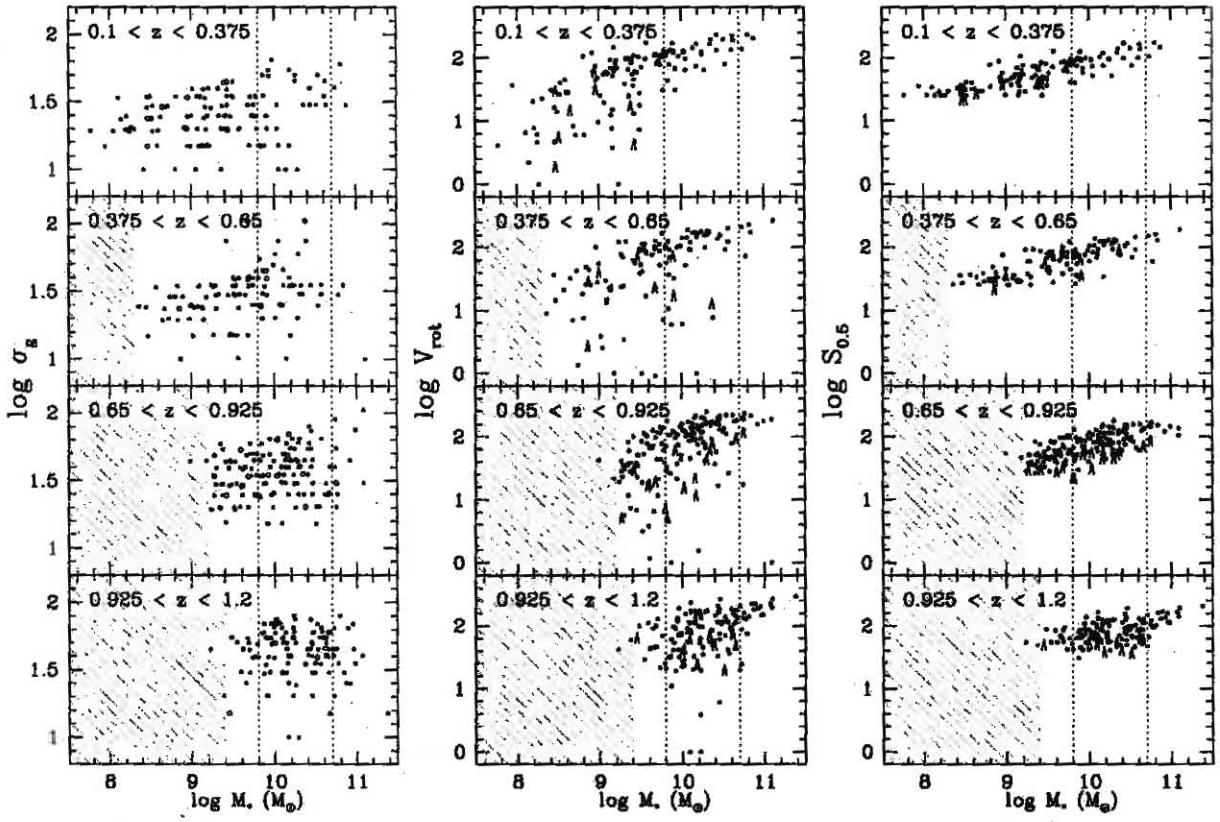

FIG. 2.— Relationships between kinematic quantities (σ_g, V_{rot}, $S_{0.5}$) and stellar mass are shown in bins of redshift for the K07 sample. While large scatter is found for the σ_g and V_{rot} relations, the $S_{0.5}$ relation is significantly tighter and does not evolve to within uncertainties since $z = 1.2$. The V_{rot} and $S_{0.5}$ relations are the same as in K07; we show the σ_g relation here for completeness. Hashed regions denote areas where the survey is not sensitive, and dotted lines demarcate the mass-complete sample used later in this paper. If a galaxy is deemed too morphologically disturbed to accurately determine an inclination (9% of the sample), V_{rot} is not inclination corrected, and the galaxy is shown as an upper limit symbol in the V_{rot} and $S_{0.5}$ plots and an open circle in the σ_g plot.

measurements adopted, and in §4 we describe how V_{rot} and σ_g are measured from emission lines in galaxy spectra. We show how V_{rot}, σ_g, and $S_{0.5}$ evolve with redshift in §5, and discuss the influence of galaxy stellar mass and size on this evolution in §6. In §7 we quantitatively define a settled disk galaxy and study their fraction with redshift. We compare our results to measurements of galaxy kinematics in the literature over $0 < z < 3.8$ in §8. Conclusions are given in §9. A ΛCDM cosmology is adopted throughout ($h = 0.7, \Omega_m = 0.3, \Omega_\Lambda = 0.7$), and all logarithms are base 10.

2. SAMPLE SELECTION

One of the main differences between this paper and most other studies of galaxy kinematics lies in how our sample is selected. Typically, constraints on galaxy morphology are applied to remove disturbed and major-merger galaxies. We instead include all galaxies with emission lines which are bright enough for us to measure kinematics from, regardless of morphology. Since disturbed morphology and disordered motions (as measured by σ_g) are correlated, removing such galaxies introduces a strong bias toward only the most rotation-dominated systems (Kassin et al. 2007). Little or no evolution in internal galaxy kinematics would be found for a sample selected in this manner. Such a sample would not be representative of galaxies at higher redshifts since they tend to have disturbed morphologies (e.g., Abraham et al. 1996; Abraham & van den Bergh 2001). Even when a strict morphological selection is loosened somewhat to include galaxies which are moderately disturbed but disk-like, still little scatter and no evolution in Tully-Fisher are found (Miller et al. 2011, 2012). Furthermore, many studies of galaxy kinematics are limited to galaxies with extremely bright emission lines. The sensitivity of DEEP2 allows us to probe a large range in galaxy stellar mass and color (Figure 1).

In addition to a broad morphological selection criterion and a large range in stellar mass, in order to study the evolution of disk galaxy kinematics over a significant look-back time, high resolution spectra of a *sizable* sample of galaxies which span a wide range in redshift are required. A sizable sample is needed because emission-line galaxies have significant intrinsic scatter in their kinematic properties (Weiner et al. 2006a,b; Kassin et al. 2007). To this end, we adopt measurements of internal galaxy kinematics for 544 galaxies from Kassin et al. (2007) (hereafter K07). This sample derives from a very large collection of 9715 galaxies with solid spectroscopic redshifts from Keck/DEIMOS (Faber et al. 2003) in field

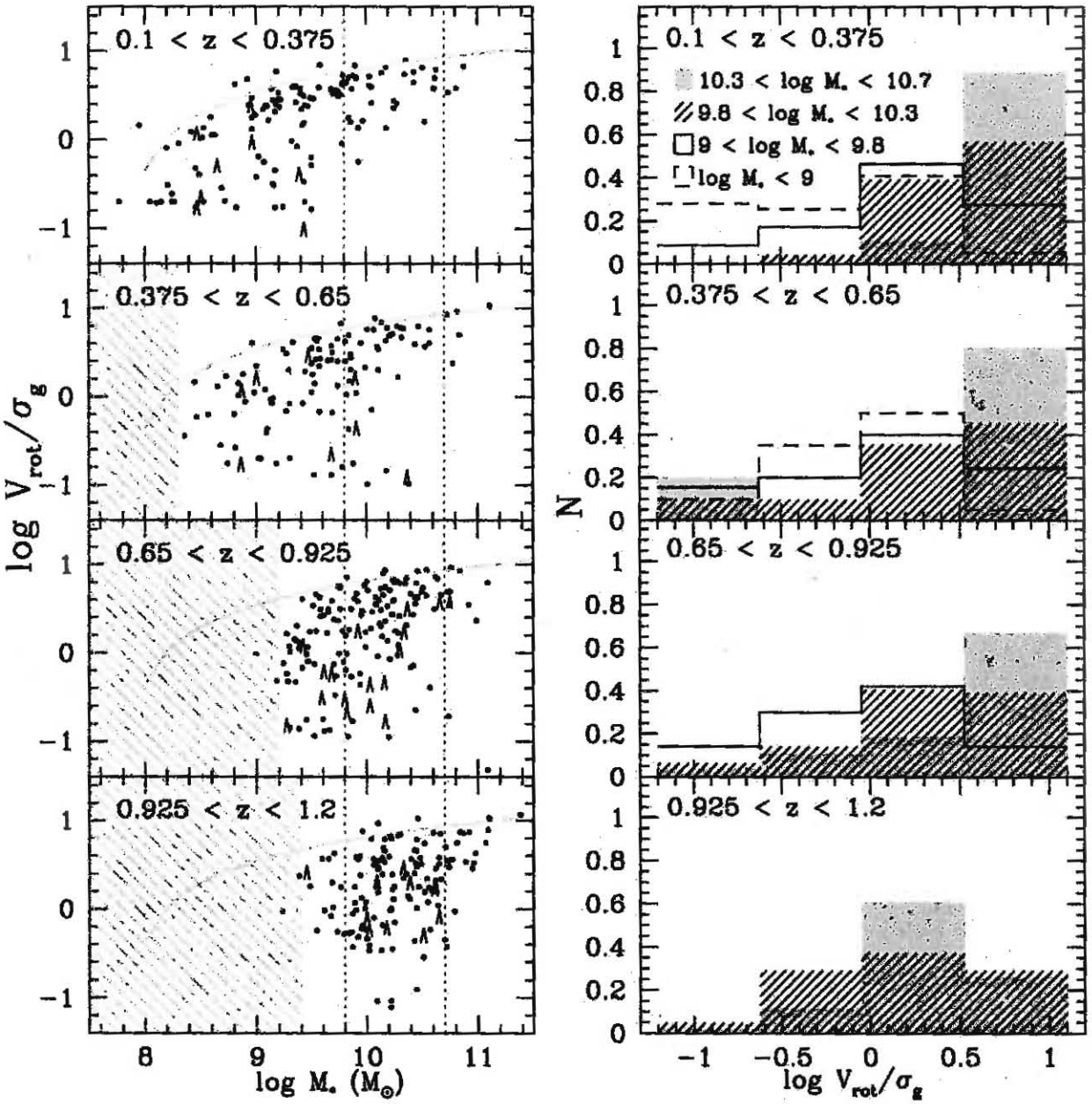

FIG. 3.— Left: The ratio of ordered to disordered motions in a galaxy, V_{rot}/σ_g, is shown as a function of stellar mass and in bins of redshift for the K07 sample. The galaxies define an upper envelope which does not evolve with redshift. However, galaxies evolve within the envelope: the lower-right corner evacuates with time (from high to low redshift), with higher mass galaxies evolving the fastest. Hashed regions denote areas where the survey is not sensitive, and dotted lines demarcate the mass-complete sample used later in this paper. Galaxy symbols are as in Figure 1. Right: This evolution is more clearly shown as histograms of V_{rot}/σ_g for galaxies divided into stellar mass bins.

1 of the DEEP2 Survey (May 2007 catalog). Galaxies in field 1 of DEEP2 are observed to a limiting magnitude of $R_{AB} < 24.1$ and are not subject to a color selection (Willmer et al. 2006). In Figure 1, we show rest-frame color-magnitude diagrams for galaxies in field 1 of DEEP2 and the K07 sample. The K07 sample traces the entire stellar mass range of the survey and a significant range in color in the "blue cloud" at all redshifts.

We now detail how galaxies were selected from field 1 of the DEEP2 Survey to be in the K07 sample. First, although the DEEP2 reaches a redshift of $z = 1.5$, K07 chose to be conservative in their selection and limit their sample to $z = 1.2$, leaving 8787 galaxies. This helps to avoid the high-redshift end of the survey where the selection is in the rest-ultraviolet and dependent on color (Willmer et al. 2006). It also avoids galaxy axes ratios

measured from *Hubble* imaging which has shifted into the ultraviolet (axes ratios are used to correct rotation velocities for inclinations of galaxies to the line-of-sight). Next, galaxies were chosen to have *Hubble Space Telescope*/ACS imaging at V and I, which further reduces the sample to 3523 galaxies. This is because there are portions of field 1 of the DEEP2 Survey which are not imaged by *Hubble*. Beside removing galaxies which did not have *Hubble* imaging, this requirement did not affect our sample selection any further because the *Hubble* images are deeper than the spectral survey. For our most important selection, galaxies with bright enough emission lines to measure kinematics ($\gtrsim 10^{-17}$ erg s^{-1} cm^2) were chosen, leaving 1692 galaxies.

Galaxies were further selected to have inclinations measured from *Hubble* images between $30° < i < 70°$, and spectrographic slits with position angles aligned to within 40° of their major axes. These cuts leave a sample of 755 galaxies. Inclinations are measured from *Hubble* images using the GIM2D software (Simard et al. 2002), as described in Dutton et al. (2011) and Cheung et al. in preparation. The inclination cut avoids nearly face-on galaxies for which inclination measurements are very uncertain, and the effects of dust in the determination of stellar mass for highly inclined systems. Inclinations are measured from the V-band *Hubble* image for galaxies at $z < 0.6$, and the I-band *Hubble* image for galaxies at $z > 0.6$. However, if the morphology of a galaxy was deemed by eye to be disturbed enough such that its inclination could not be reliably determined, it was included in the sample but not corrected for inclination. There are only 24 of these galaxies and they are flagged in the following analysis. Removing them from the sample does not significantly affect the results of this paper. For the slit position angles, due to the large slit width (1″) compared to the apparent sizes of galaxies in our sample ($\sim 3''$), seeing will allow us to measure accurate kinematics when slits have position angles which are offset by up to 40° from galaxy major axes (see Figure 13 of Weiner et al. 2006a). Finally, if an emission line was affected by a sky line or instrumental artifact, we removed the corresponding galaxy from the sample, leaving a total of 544 galaxies in the K07 sample. No constraints on morphology were ever applied.

To study the evolution of galaxy kinematics for a sample which is mass-complete at all redshifts, in §5.1 we will limit the K07 sample to galaxies with stellar masses (M_*) over $9.8 < \log M_*(M_\odot) < 10.7$, as demarcated in Figures 1–3. Since the M_* function of blue galaxies does not evolve significantly since $z \sim 1$ (Borch et al. 2006; Bundy et al. 2006; Pozzetti et al. 2010), we do not change this M_* range with redshift. This cut removes 274 galaxies from the K07 sample, leaving 270. Throughout the paper we will refer to this as the "mass-complete sample."

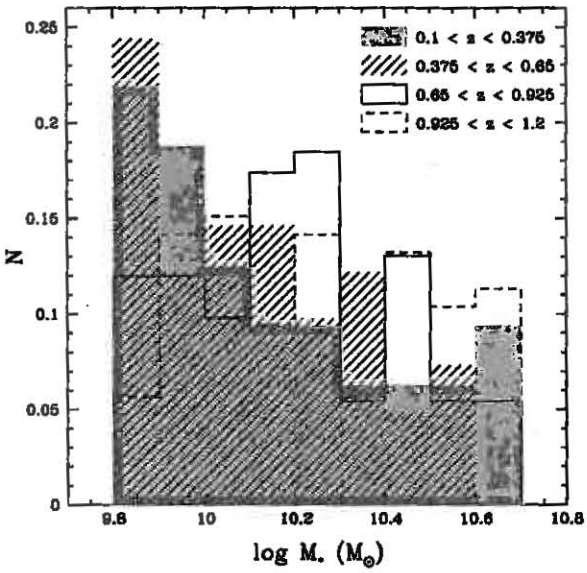

FIG. 4.— For the mass-complete sample, the distribution of galaxy stellar masses among the redshift bins in Figure 3 is shown. It demonstrates a bias in the lower redshift bins towards lower stellar masses, and a bias in the higher redshift bins towards higher stellar masses. *These biases work in the opposite direction to our results, making our results lower limits to the intrinsic evolution.*

3. STELLAR MASS AND SIZE MEASUREMENTS

In this paper, we study the relationship between galaxy kinematics and M_*. We adopt M_* measurements from Bundy et al. (2006) who performed fits of galaxy stellar population models to observed B, R, I, and K_s-band integrated galaxy fluxes. The models constituted a grid of synthetic spectral energy distributions from Bruzual & Charlot (2003) which spanned a range of exponential star-formation histories, ages (restricted to be less than the age of the Universe at the redshifts of the galaxies), metallicities, and dust contents. A Chabrier (2003) initial mass function was adopted. For a given galaxy, at each point on the grid of models, the following was calculated: the minimum χ^2, probability that each model accurately describes the galaxy, and the K_s-band stellar mass-to-light ratio. The corresponding M_* at each point was then determined by scaling the stellar mass-to-light ratio to the K_s-band luminosity. The probabilities were then summed (marginalised) across the grid and binned by model M_*, which yielded a M_* probability distribution for the galaxy. The median of the distribution was adopted as the best estimate. The M_*'s measured in this way are robust to degeneracies in the models, such as those between age and metallicity. The uncertainties in these M_* measurements are ~ 0.2 dex.

In addition to the effects of M_* on galaxy kinematics, we also look to galaxy sizes. Two size measurements are studied: emission line extents and continuum sizes. Emission line extents are measured from the ground-based DEEP2 spectra from the same lines used to measure kinematics. However, unlike the kinematics measurements, seeing is not corrected for. We measure the spatial extent of the line emission as follows. For details on the method, see Weiner et al. (2006a). First, we measure the spectral continuum by collapsing the two-dimensional spectra in wavelength over a 15Å range around the line and two 100Å spatial ranges on either side of the line. We then fit Gaussian profiles along the slit using a non-linear least-squares routine, and tabulate the resulting full-width-half-maxima (FWHM), which we adopt as our measurement of emission line extent. Our other size measurements, galaxy continuum sizes, are

measured from *Hubble* images, and are therefore unaffected by seeing. To take into account band-shifting with redshift, sizes are measured from the V and I-band images for galaxies at redshifts less than and greater than 0.6, respectively. The images are of one-orbit depth and reach 28.75 and 28.10 AB magnitudes (5σ) for V and I, respectively. Measurements of galaxy half-light radii are made with the GIM2D software (Simard et al. 2002), as described in Dutton et al. (2011) and Cheung et al. in preparation.

4. KINEMATIC MEASUREMENTS

In this section, we describe the measurements of internal galaxy kinematics from emission lines which we adopt from K07. Details on how these measurements were made are in Weiner et al. (2006a) for a similar survey with the same telescope/instrument, but at lower spectral resolution ($R \sim 2100$ versus $R \sim 5000$). The emission line used to measure kinematics is the one with the highest signal-to-noise in the galaxy spectrum. For the vast majority of galaxies, the Hα λ6563, [O II] $\lambda\lambda$3726.0,3728.8, and [O III] λ5007 lines are used. Rotation velocities on the flat part of the rotation curves ($V_{rot} \times sin(i)$, where i is the inclination of a galaxy to the line-of-sight) and integrated gas velocity dispersions (σ_g) were measured simultaneously from emission lines in the spectra, and the effects of seeing (typically $\sim 0.7''$) were taken into account. Our high spectral resolution allows for V_{rot} and σ_g to be measured down to ~ 5 and ~ 10 km s^{-1}, respectively, if present. An uncertainty of 10 km s^{-1} is adopted for both σ_g and the inclination-corrected V_{rot} to account for random errors and the dependence of the model parameters on the assumed seeing and scale radius of the rotation curve. Although many of the rotation curves do not "turn over" due to seeing, our model is still able to fit for V_{rot}. It has been demonstrated using data with the same telescope/instrument which reach the turn-over radius for 90% of galaxies, that spectra of our depth do not show a bias in V_{rot} (Figure 6 of Miller et al. 2011). However, benefits of the deeper data are smaller errors in $V_{rot} \times sin(i)$ (and therefore less scatter) and the ability to probe galaxies with fainter emission lines (Miller et al. 2011). Except for the 24 galaxies for which reliable inclinations could not be determined (§2), values of $V_{rot} \times sin(i)$ are corrected for galaxy inclinations measured from the *Hubble* images. The results of this paper do not change significantly if these 24 galaxies are removed from the sample.

4.1. *What σ_g and V_{rot} Measure*

The integrated gas velocity dispersion we measure (σ_g) is unlike the typical pressure-supported velocity dispersion measured for early type galaxies or galaxy bulges. This is the case for two reasons. First, σ_g is measured from emission lines which trace the gas in galaxies, as opposed to absorption lines which trace stars. Gas, unlike the collisionless stars in an early type galaxy, can dissipate energy and therefore cannot remain in a high dispersion equilibrium state with crossing orbits. Secondly, because the spectral slits used in the DEEP2 Survey are wide compared to the apparent sizes of the galaxies observed ($1''$ slit vs. $\sim 3''$ galaxies), σ_g effectively integrates velocity gradients on scales at and below the seeing limit (Weiner et al. 2006a; Covington et al. 2010; Epinat et al. 2010). For values of σ_g less than ~ 35 km s^{-1}, which is the upper limit for well-ordered disk galaxies in the local Universe (Figure 15 of Epinat et al. 2010), σ_g measures the relative motions of individual star-forming regions in galaxy disks. However, for values of σ_g greater than ~ 35 km s^{-1}, σ_g integrates over velocity gradients which can correspond to non-ordered gas kinematics such as small-scale velocity gradients, gas motions due to star-formation, or superimposed clumps along the line of sight. *In this paper, we collectively refer to these velocity gradients as "disturbed motions."*

To test for interference from V_{rot} in measurements of σ_g, in §5 we compare σ_g measured for galaxies in our mass-complete sample with galaxies from DEEP2 which are face-on in *Hubble* images (i.e., $i < 30°$) and in the same M_* range. We find no significant difference in the trend of σ_g with redshift between these two samples, making it unlikely that the V_{rot} of a galaxy interferes with the measurement of σ_g.

To further investigate what σ_g and V_{rot} measure, in Covington et al. (2010) we performed mock observations of a suite of galaxy merger simulations. These simulations provided model galaxies in various stages of disorder, ranging the gamut from well-ordered disks to merger remnants. The mock observations were performed just as the actual observations. Galaxies were redshifted to $z \sim 0.3$ and $z \sim 1.0$, and seeing, slit width, and detector pixel size were taken into account. Our algorithm for fitting kinematics was found by Covington et al. (2010) to be successful at reproducing σ_g, but was found to underestimate values of V_{rot} by up to 30%, independent of a merger stage or redshift. However, as we note in §2, Miller et al. (2011) compared measurements of V_{rot} for data similar to ours with deeper data which reach the turn-over radius, and do not find a systematic offset in V_{rot} between the two measurements. Therefore, if we are underestimating V_{rot}, we are probably not doing so significantly.

5. EVOLUTION OF GALAXY KINEMATICS

In this section, we examine how the kinematics of blue galaxies evolve with redshift. First we examine the full K07 sample, and then we study a mass-complete subsample.

5.1. *The Full K07 Sample*

In Figure 2, we show σ_g, V_{rot}, and $S_{0.5}$ versus M_* in bins of redshift for the K07 sample. The V_{rot} versus M_* relation (i.e., the stellar mass Tully-Fisher Relation) shows large scatter to low V_{rot} (K07). The σ_g versus M_* relation also shows significant scatter in σ_g. However, when V_{rot} and σ_g are combined into $S_{0.5}$, the resulting relation with M_* tightens significantly and does not evolve with redshift to within uncertainties (K07). The quantity $S_{0.5}$ is a tracer of potential well depth (Weiner et al. 2006a; Kassin et al. 2007). Figure 2 also shows that at lower redshifts, higher mass galaxies have on average larger values of V_{rot} and smaller values of σ_g than at higher redshift. It is also clear from this figure that at lower redshift, lower mass galaxies have low values of V_{rot} and high values of σ_g; they are too faint to be observed at higher redshifts in our survey.

These findings are illustrated more clearly in Figure 3 (left column) where the quantity V_{rot}/σ_g, the ratio of

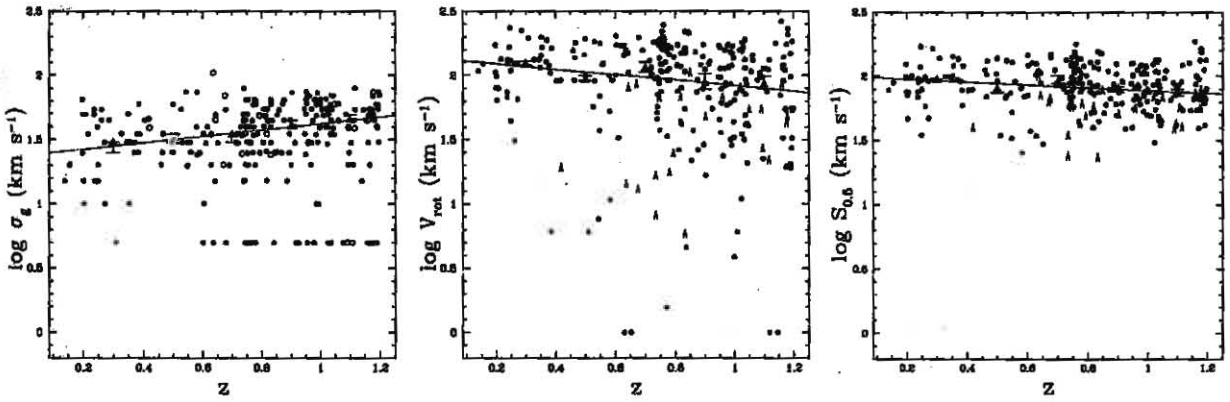

FIG. 5.— The evolution of σ_g, V_{rot}, and $S_{0.5} \equiv \sqrt{0.5V_{rot}^2 + \sigma_g^2}$ with redshift for the mass-complete sample ($9.8 < \log M_*(M_\odot) < 10.7$) is shown. Galaxies increase in σ_g, and decrease in V_{rot} and $S_{0.5}$ with increasing redshift. Galaxies are plotted as black symbols, as described in Figure 1. Binned medians are shown as red triangles with error bars representing the error on the medians determined by bootstrap re-sampling the data. Linear fits to the binned medians are shown as red solid lines.

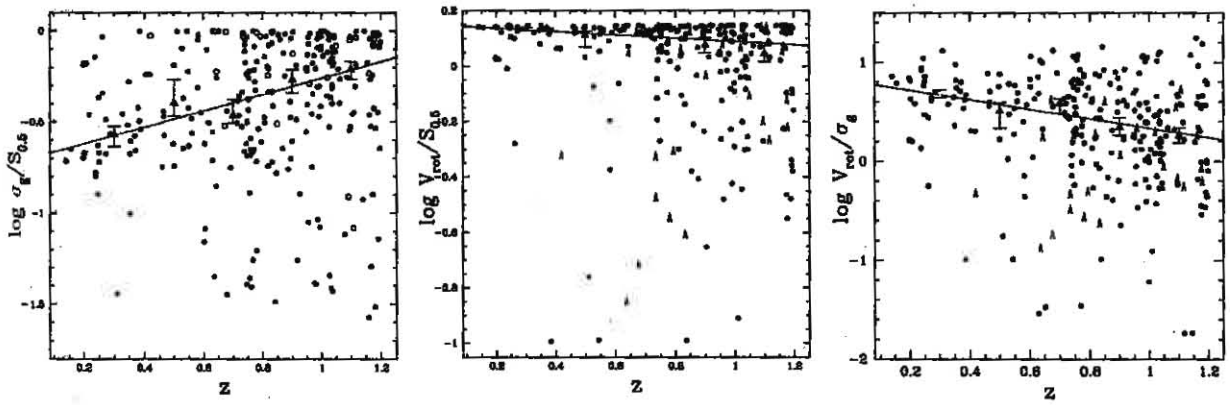

FIG. 6.— The evolution of $\sigma_g/S_{0.5}$, $V_{rot}/S_{0.5}$, and V_{rot}/σ_g with redshift for the mass-complete sample is shown. The first two of these ratios remove the dependence on potential well depth (i.e., $S_{0.5}$) in the σ_g and V_{rot} plots in Figure 5. Symbols, error bars, and fits are the same as in Figure 5.

ordered to disordered motions in a galaxy, is plotted versus M_* in bins of redshift.[12] The galaxies define an upper envelope in V_{rot}/σ_g versus M_*-space which does not evolve since $z = 1.2$. However, galaxies evolve within the envelope: with increasing time they move away from the bottom of the plot toward the upper envelope, and this happens first for massive galaxies. This evolution is better quantified by the histograms in Figure 3 (right column) which demonstrate that galaxies move towards higher V_{rot}/σ_g decreasing redshift (i.e., with time), and the highest mass galaxies have on average the highest values of V_{rot}/σ_g at all times.

5.2. *A Mass-Complete Galaxy Sample*

To investigate this trend of V_{rot}/σ_g with redshift for all but the very lowest and very highest mass galaxies in our sample, we create a mass-complete sample by selecting galaxies with stellar masses over $9.8 < \log M_*(M_\odot) < 10.7$ (vertical dotted lines in Figures 1-3). For this subsection and for §6, we will focus on this mass-complete sample of 270 galaxies, unless noted. In Figure 4, for the mass-complete sample, we show the distribution of galaxy M_* among the redshift bins in Figure 3. It illustrates that the lower redshift bins are biased towards lower mass galaxies, and the higher redshift bins towards higher mass galaxies. *These biases work in the opposite direction to our results. Therefore, the evolution we find is interpreted as a lower limit to the intrinsic evolution.*

Figure 5 shows the evolution of σ_g, V_{rot} and $S_{0.5}$ with redshift for the mass-complete sample. All three quantities have large intrinsic scatter. We will demonstrate that a portion of the scatter for V_{rot} and σ_g is due to M_*, or size, in §6. We fit linear relations to each of the quantities versus redshift by performing linear least-squares fits to the binned medians in Figure 5. The medians are zero-pointed near the middle of the sample to avoid covariances. Of the three quantities, σ_g shows the strongest evolution (5.0σ). It increases linearly with redshift to $z = 1.2$ (i.e., decreases with time) as

$$log\ \sigma_g - 0.42 = (0.25 \pm 0.05)(z - 0.82) + (1.16 \pm 0.01). \quad (1)$$

The median increases from 27 ± 1 km s^{-1} at $z = 0.2$ to

[12] In the evaluation of V_{rot}/σ_g, a minimum value of σ_g of 15 km s^{-1} is adopted to avoid dividing by small numbers with relatively large uncertainties.

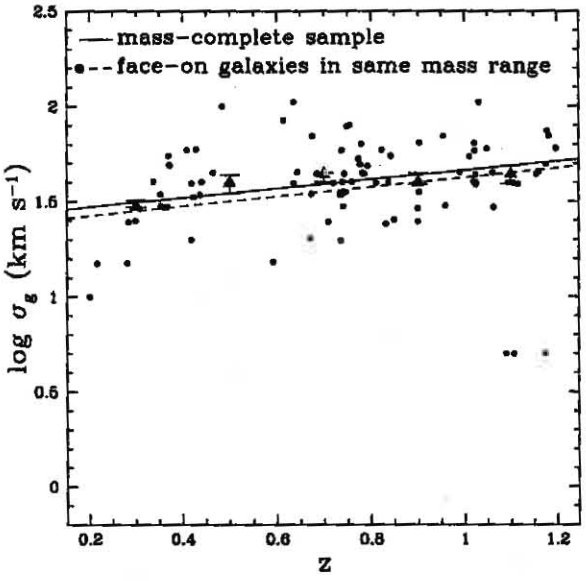

FIG. 7.— The evolution of σ_g with redshift for galaxies oriented face-on in *Hubble* images ($i < 30°$) is compared with that for galaxies in the mass-complete sample from Figure 5, and is not found to be significantly different. The solid line is a fit to the face-on galaxies, and the dashed line is the fit to the mass-complete sample. Both samples span the same M_* range, and both fits are given in the text. Symbols and error bars are as in Figure 5.

47 ± 1 km s^{-1} at $z = 1.2$. The quantity which shows the second-most strongest evolution is V_{rot} (4.2σ). It decreases with redshift as

$$log\ V_{rot} - 2.00 = (-0.21 \pm 0.05)(z - 0.82) - (0.04 \pm 0.02). \quad (2)$$

The median decreases from 123 ± 1 km s^{-1} at $z = 0.2$ to 76 ± 1 km s^{-1} at $z = 1.2$. Finally, the quantity $S_{0.5}$ shows the weakest evolution of the three (3.6σ). It decreases with redshift as

$$log\ S_{0.5} - 1.92 = (-0.11 \pm 0.04)(z - 0.82) + (0.00 \pm 0.01). \quad (3)$$

The median decreases from 97 ± 1 km s^{-1} at $z = 0.2$ to 75 ± 1 km s^{-1} at $z = 1.2$.

Some of the evolution found for these three quantities, may be due to a changing distribution of galaxy masses in the sample with time. This can be caused by galaxies growing in mass and/or high mass galaxies quenching their star-formation and leaving the sample. To address this for σ_g and V_{rot}, we remove the dependence on potential well depth by examining ratios with $S_{0.5}$, namely $\sigma_g/S_{0.5}$ and $V_{rot}/S_{0.5}$. These ratios are shown as a function of redshift in Figure 6. They express the fraction of kinematic support which comes from ordered or disordered motions. The ratio $\sigma_g/S_{0.5}$ increases with redshift (5.0σ) as

$$log\ \sigma_g/S_{0.5} + 0.35 = (0.45 \pm 0.09)(z - 0.82) + (0.01 \pm 0.03), \quad (4)$$

and the ratio $V_{rot}/S_{0.5}$ decreases with redshift (3.0σ) as

$$log\ V_{rot}/S_{0.5} - 0.10 = (-0.06 \pm 0.02)(z - 0.82) + (0.00 \pm 0.01). \quad (5)$$

As before, these are linear least-squares fits to the median points in Figure 6. These ratios demonstrate that the increasing role of σ_g and the declining role of V_{rot} with increasing redshift are not due to a changing distribution of galaxy masses in the sample with time.

In addition to ratios with $S_{0.5}$, we look to V_{rot}/σ_g, the ratio of ordered to disordered motions, with redshift[12]. This is not an ideal quantity since neither V_{rot} nor σ_g is constant with redshift. In addition, σ_g is a small number with a proportionally large uncertainty, and dividing by it contributes significantly to the scatter in V_{rot}/σ_g. Nevertheless, due to the significant trends of σ_g and V_{rot} with redshift, V_{rot}/σ_g shows strong evolution (4.8σ; Figure 6):

$$log\ V_{rot}/\sigma_g - 1.55 = (-0.48 \pm 0.10)(z - 0.82) - (1.13 \pm 0.04). \quad (6)$$

To determine whether the V_{rot} of a galaxy influences our measurements of σ_g, in Figure 7 we examine how σ_g evolves with redshift for galaxies from the DEEP2 Survey which are face-on in *Hubble* images (i.e., $i \leq 30°$) and in the same stellar mass range as the mass-complete sample. We find same evolution to within uncertainties for face-on galaxies: $log\ \sigma_g - 0.42 = (0.24 \pm 0.04)(z - 0.82) + (1.20 \pm 0.02)$, demonstrating that V_{rot} does not influence our measurements of σ_g.

6. DOWNSIZING

In this section, we demonstrate that much of the scatter in the relations of $\sigma_g/S_{0.5}$ and $V_{rot}/S_{0.5}$ with redshift is attributable to galaxy properties such as M_* and size. We find that trends with M_* and size are of similar strengths.

First we consider M_*. In Figure 8, as in Figure 6, we show $\sigma_g/S_{0.5}$ and $V_{rot}/S_{0.5}$ as a function of redshift for the mass-complete sample. However, in Figure 8, galaxies are divided into two M_* bins: $9.8 < \log M_*(M_\odot) < 10.3$ and $10.3 < \log M_*(M_\odot) < 10.7$. Similar trends to those found for the entire mass-complete sample are also found separately for the low and high mass galaxies. It is also clear from Figure 8 that, at all redshifts, higher mass galaxies are more kinematically settled (i.e., higher V_{rot} and lower σ_g) than lower mass galaxies. This is consistent with downsizing trends (e.g., Cowie et al. 1996), and we refer to this phenomenon as "kinematic downsizing."

Next we examine trends with size. We consider two size measurements: *Hubble* continuum sizes and emission line extents, as described in §3. *Hubble* sizes are unaffected by seeing, and emission line extents are affected by seeing and are *not* corrected for it. Figure 9 is similar to Figure 8, except galaxies are color-coded according to size instead of M_*. For both size measurements, three size bins are shown: < 3.5 kpc, 3.5–5 kpc, and > 5 kpc. Figure 9 shows that on average, at all redshifts, the largest galaxies are the most kinematically well-ordered, the smallest the most disordered, and intermediate-sized galaxies have properties in between the large and small galaxies. This is the case for both size measurements. It demonstrates that the emission lines, which we use to measure galaxy kinematics, trace the galaxy continua well, and that we are able to measure reliable rotation velocities for the small galaxies in our sample.

Figures 8 and 9 also demonstrate that the evolution in Figures 5 and 6 is not due to a special population of high-redshift galaxies with high values of σ_g and low values of V_{rot}. It occurs even if only massive/large galaxies are considered.

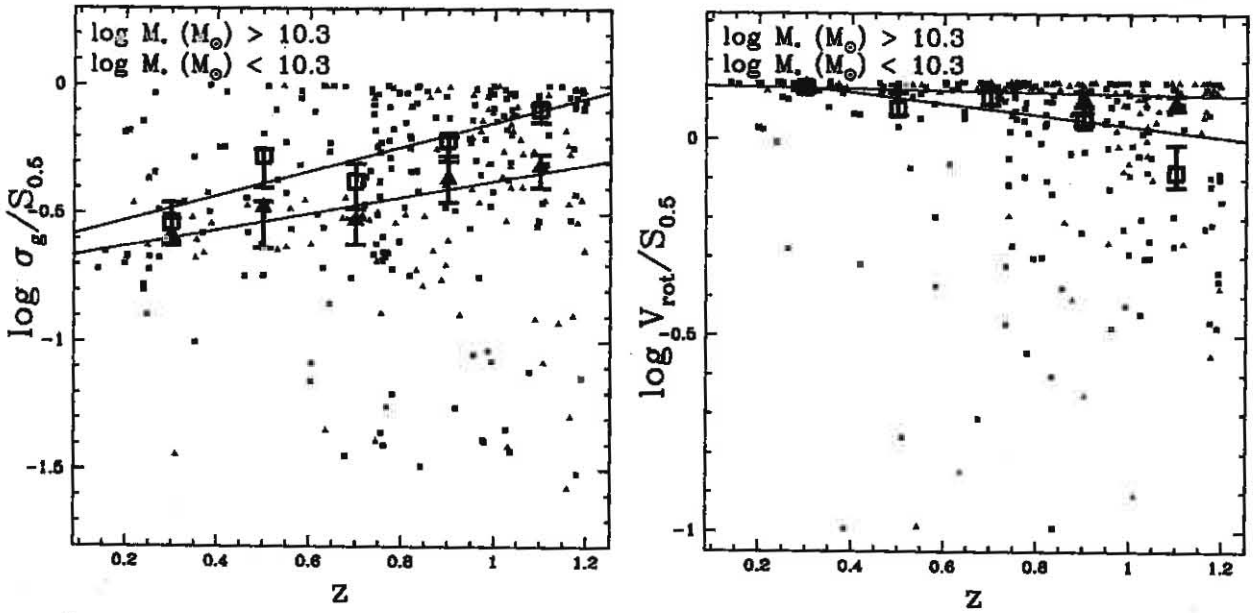

FIG. 8.— As in Figure 6, the quantities $\sigma_g/S_{0.5}$ and $V_{rot}/S_{0.5}$ are shown as a function of redshift, but here galaxies are divided into two mass bins: log $M_* < 10.3$ (low mass, black squares) and log $M_* > 10.3$ (high mass, red triangles). Both mass ranges show similar trends with redshift as the full mass-complete sample, but the higher mass galaxies are the most well-ordered at all redshifts (high $V_{rot}/S_{0.5}$ and low $\sigma_g/S_{0.5}$). Error bars and fits are the same as in Figure 5.

7. SETTLING FRACTION

To better quantify how blue galaxies evolve in σ_g and V_{rot}, we use these parameters to define a kinematically settled disk galaxy, and study the fraction of settled disk galaxies as a function of M_* and redshift. For the definition, we first look to the distribution of V_{rot}/σ_g in Figure 3 and then to *Hubble* morphologies. Since we regard higher mass blue galaxies to be on average kinematically settled disks at low redshift, we look to their values of V_{rot}/σ_g in Figure 3. A typical value for galaxies with log $M_*(M_\odot) > 9.8$ is ~ 3 (i.e., log $V_{rot}/\sigma_g = 0.48$). We now consider *Hubble* morphologies. Kassin et al. in preparation show that *Hubble* morphologies are correlated with V_{rot}/σ_g such that galaxies with normal morphologies have higher values than galaxies with disturbed morphologies. We find that $V_{rot}/\sigma_g \sim 3$ provides a reasonable division between normal and disturbed morphologies, as demonstrated by the *Hubble* images of 6 example galaxies from the K07 sample in Figure 10.

Now that we have a quantitative definition of a settled disk galaxy (i.e., $V_{rot}/\sigma_g > 3$), we use it to study the fraction of blue galaxies which are settled, f_{settle}. The evolution of f_{settle} with redshift for the full K07 sample divided into in four M_* bins is shown in Figure 11. All bins except for the lowest mass bin show decreasing f_{settle} with increasing redshift (i.e., increasing f_{settle} with time). It decreases from $38 - 24\%$, $57 - 31\%$, and $89 - 33\%$ since $z = 1.2$ for mass bins of $9.0 < \log M_*(M_\odot) < 9.8$, $9.8 < \log M_*(M_\odot) < 10.3$, and $10.3 < \log M_*(M_\odot) < 10.7$. These results are lower limits to the intrinsic evolution due to biases towards low/high mass galaxies in low/high redshift bins (Figure 4). Furthermore, at all redshifts, the higher the M_* of the population, the higher its f_{settle}. The same qualitative behavior is found for settled galaxies defined as having values of V_{rot}/σ_g between 1 and 5.

8. KINEMATIC MEASUREMENTS IN THE LITERATURE

In this section, we compare our measurements with those in the literature for local galaxies, and for galaxies at similar redshifts. We also compile kinematic measurements from the literature for galaxies at higher redshifts. Measurements of $S_{0.5}$, V_{rot}, and σ_g from the literature are shown in Figure 12. All are from IFS observations. In the panels on the left and right, galaxies are color-coded according to stellar mass (for a Chabrier 2003 initial mass function) and emission-line extent, respectively, unless noted in the text below. Here we detail the measurements adopted from the literature in order of increasing redshift, and note if they differ from measurements used in this paper.

To compare our results with local galaxies, a large homogenous sample is needed, and the GHASP survey (Epinat et al. 2010) provides just this. In Figure 12, we show the median values of $S_{0.5}$, V_{rot}, and σ_g for galaxies in GHASP. Error bars on the median points show the rms scatter. GHASP spans a larger range in stellar masses than our sample: $9.0 < \log M_*(M_\odot) < 11.7$ for a 'diet' Salpeter IMF (Epinat et al. 2008), which is roughly 0.15 dex higher than the Chabrier (2003) IMF used in this paper. Regardless, the median values are consistent with extrapolations of our relations to $z = 0$.

In Figure 12, kinematics measurements for 68 galaxies from the IMAGES IFS Survey with a median redshift of 0.6 are shown (Puech private comunication, Puech et al. 2008, Neichel et al. 2009). The sizes used are continuum half-light radii. Although galaxies in IMAGES are selected to be representative of galaxies with $M_* \geq 1.5 \times 10^{10}$ M$_\odot$ at $0.4 < z < 0.75$ (Yang et al.

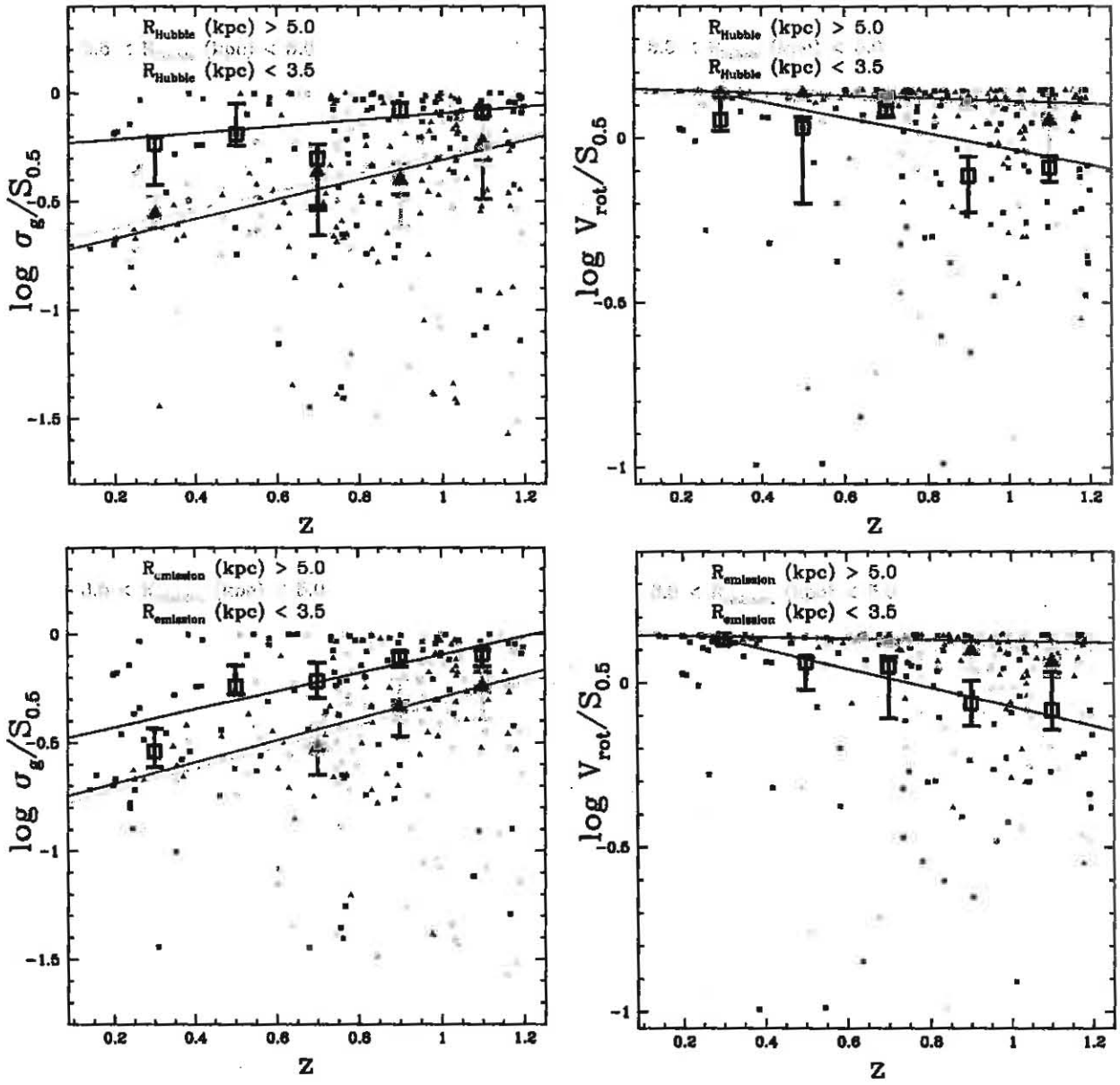

FIG. 9.— This figure is the same as Figure 8, except galaxies are divided into three size bins: < 3.5 kpc (black squares), 3.5–5 kpc (grey circles), and > 5 kpc (red triangles). Two sizes are considered: *Hubble* half-light radius (top; which is not affected by seeing), and emission line extent (bottom; which is affected by seeing and not corrected for its influence). Galaxies in size bins show similar trends to the full mass-complete sample. At all redshifts, the largest galaxies are the most well-ordered (i.e., high $V_{rot}/S_{0.5}$, low $\sigma_g/S_{0.5}$), the intermediate-sized galaxies the next well-ordered, and the smallest galaxies the least well-ordered. Error bars and fits are the same as in Figure 5. For the *Hubble* continuum sizes, there is a deviation from the trends in the $z = 0.7$ bin because this is where we switch from using the V-band to the I-band for the size measurements.

2008), similar to our selection, the median V_{rot} and σ_g of IMAGES galaxies are larger than ours at $z = 0.6$ by 0.22 and 0.19 dex, respectively. It is possible that the median V_{rot} is higher likely because the limited spatial coverage of the IFS may have caused V_{rot} to be overestimated (Puech et al. 2008). This especially seems to be the case for the smaller galaxies (< 3 kpc). The median σ_g is higher because, unlike our procedure of fitting for V_{rot} and σ_g simultaneously, they are fit separately in IMAGES. Therefore, to derive an average σ_g from the velocity dispersion field of a galaxy, pixels affected by the seeing-induced peak at the center of a galaxy are ignored and σ_g is taken as the signal-to-noise weighted mean of the remaining pixels in the outer parts (Puech et al. 2007). This may result in σ_g measurements which are biased high because pixels with the highest signal-to-noise are ignored (e.g., Davies et al. 2011).

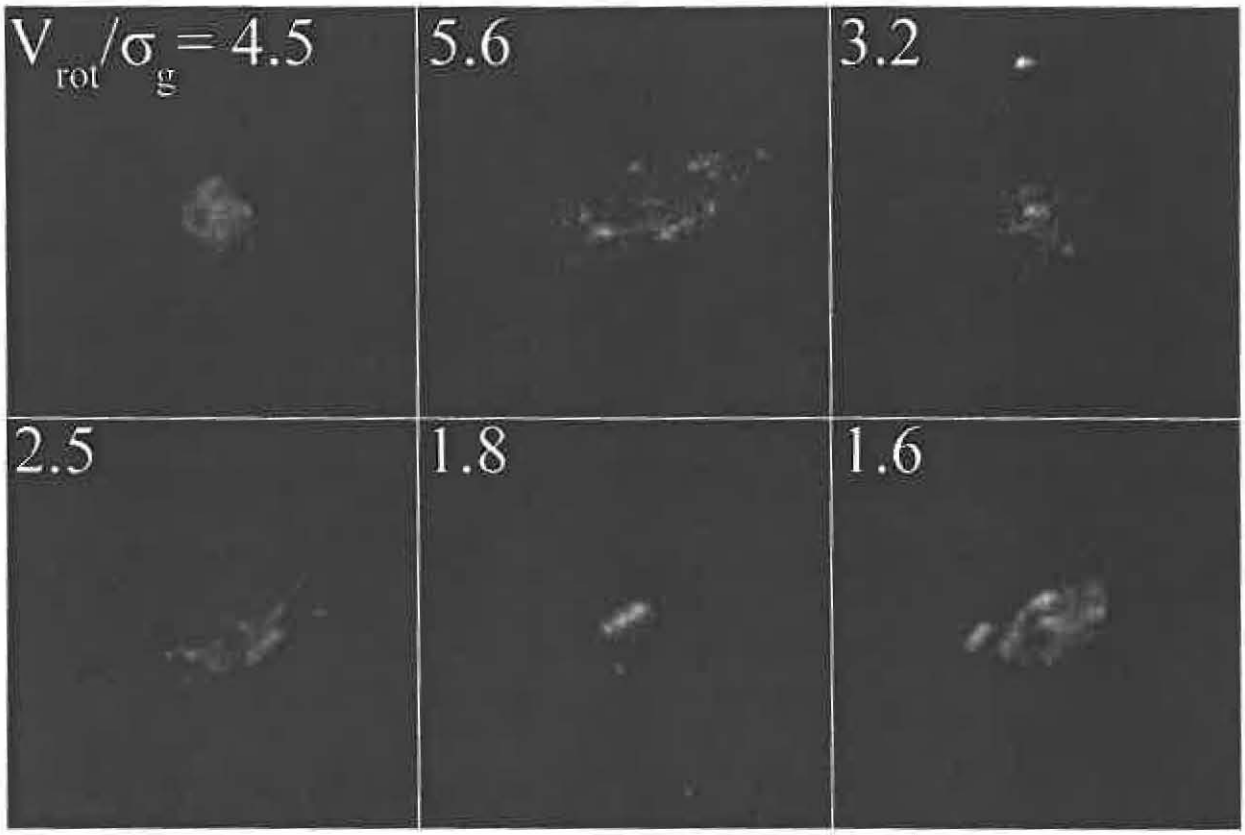

FIG. 10.— *Hubble/ACS* $V+I$ images of settled (top) and unsettled (bottom) galaxies which are defined as having $V_{rot}/\sigma_g > 3$ and $V_{rot}/\sigma_g < 3$, respectively. The settled galaxies have normal morphologies, and the unsettled galaxies have disturbed morphologies (Kassin et al. in preparation). All galaxies are at $z = 1$ and have stellar masses in the range $10.4 < \log M_*(M_\odot) < 11.1$. The images are 6″ on a side.

8.1. *Kinematic Measurements at* $1.2 < z < 3.8$

Kinematics are difficult to obtain for galaxies at $z \gtrsim 1.2$ since emission lines are redshifted to near-infrared wavelengths where the sky is bright in continuum and line emission, making spectroscopy difficult. Nevertheless, pioneering studies of galaxy kinematics at $z \gtrsim 1.2$ with single-slit spectrographs gave the first glimpse of the kinematic state of galaxies at these earlier times, albeit only the most highly star-forming systems (e.g., Erb et al. 2004, 2006). More recently, there has been a boom in IFS observations of galaxy kinematics at these redshifts. Unfortunately, to obtain enough signal-to-noise to measure kinematics in a reasonable amount of observing time, all samples at these redshifts are still biased toward galaxies with the brightest emission lines, which are the most highly star-forming systems.

Many galaxies at $z \gtrsim 1.2$ have kinematics which were unable to be fit by a rotating disk model (either due to low signal-to-noise, small spatial extent, or a non-ordered velocity field). For these galaxies, we adopt as a rotation velocity in Figure 12 half of the velocity shear across the face of the galaxy ($\frac{1}{2} \times V_{shear}$). The quantity V_{shear} is the difference between the minimum and maximum rotation velocities, and is not corrected for inclination. These galaxies are shown as small filled points in Figure 12.

In Figure 12, kinematic measurements for 46 galaxies with a median redshift of 1.2 from the MASSIV Survey are shown (Contini et al. 2012; Vergani et al. 2012). Galaxies in MASSIV were selected to have very bright emission lines, and a lower-limit on emission linewidth was imposed (25Å for 42 galaxies and 40Å for 22 galaxies; Contini et al. 2012). MASSIV galaxies have a median value of σ_g which is consistent with our data, but higher median values of V_{rot} and $S_{0.5}$. The difference is likely due to the sample selection.

For 8 galaxies at $z \sim 1.5$, we adopt measurements from Wright et al. private communication for data in Wright et al. (2007) and Wright et al. (2009). All dual-component galaxies are treated as individual systems. Four of these galaxies were able to be modeled as rotating disks, and four were not. For galaxies which were able to be modeled, values of V_{rot} are *not* corrected for galaxy inclinations. For an additional 8 galaxies at $z \sim 1.5$, we adopt data from Lemoine-Busserolle & Lamareille (2010); all are modeled as rotating disks. For galaxies at $z \sim 2$, data are adopted from the SINS Survey via private communication from N. Forster-Schreiber for the most recent models and data for galaxies in Genzel et al. (2008), Förster-Schreiber et al. (2009), and Cresci et al. (2009). A total of 14 SINS galaxies were able to be modeled as rotating disks, and 33 were not. For galaxies from SINS which were not able to be modeled, we esti-

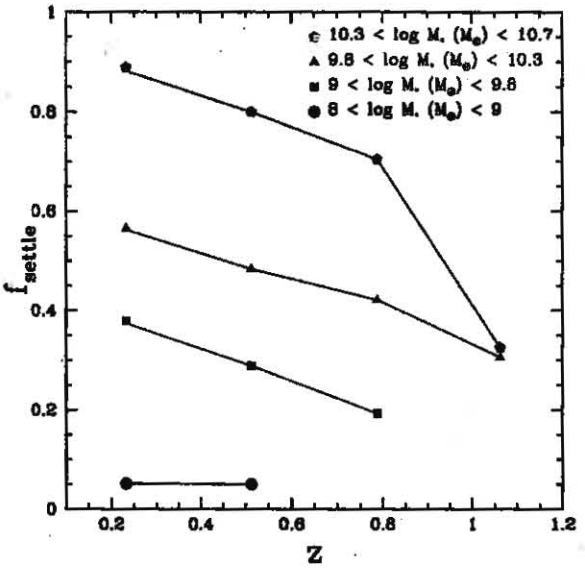

FIG. 11.— The fraction of galaxies in the full K07 sample which are settled (defined as $V_{rot}/\sigma_g > 3$), f_{settle}, is shown as a function of redshift for different stellar mass bins. The quantity f_{settle} decreases with redshift (increases with time) for all but the lowest mass bin. At all redshifts, the higher the stellar mass of the population, the higher its f_{settle}.

mate σ_g as the line-width less the velocity shear (i.e., v_{obs} from Förster-Schreiber et al. 2009 - V_{shear}). For an additional 16 systems at $z \sim 2$, none of which were able to be modeled as a rotating disk, we adopt data from Law et al. (2009). Three of the galaxies from Law et al. (2009) which have dual-components are considered as separate systems here. For 4 galaxies at $z \sim 3$, data are adopted from Lemoine-Busserolle et al. (2010); 3 are modeled as rotating disks and 1 is not. In addition, at $z \sim 3$, 12 galaxies which were modeled as disks and 7 which were not, are adopted from from the AMAZE/LSD Survey via private communication from A. Gnerucci for data from Gnerucci (2011) and Troncoso et al. in preparation.

Summary

For measurements in the literature over $1.2 < z < 3.8$, there is a large scatter in kinematic parameters and no clear trends with redshift. This is likely due to sample selection since currently only the brightest systems at these redshifts can be observed in reasonable amounts of observing time. In addition, many of the higher redshift galaxies are expected to merge and become early-type galaxies by at least today, inducing a "progenitor bias."

These data demonstrate that there exist galaxies at earlier times with rotation velocities similar to local galaxies. However, they differ from local galaxies due to large values of σ_g (e.g., Förster-Schreiber et al. 2009; Lemoine-Busserolle & Lamareille 2010; Lemoine-Busserolle et al. 2010; Gnerucci 2011; Vergani et al. 2012). The data from the literature also show the existence of a population of higher redshift galaxies with small sizes and little or no discernible rotation, but with significant values of σ_g and generally small sizes (Law et al. 2009; Förster-Schreiber et al. 2009). Although some observations at $z \sim 2$ may be too shallow to detect the full rotation gradients (Law et al. 2009; Förster-Schreiber et al. 2009), until these smaller galaxies can be observed with significantly longer exposure times to detect possible faint disks, whether they have a significant V_{rot} is unknown. Of the galaxies modeled as rotating disks at $1.2 < z < 3.0$, the more massive systems generally have higher values of V_{rot} and $S_{0.5}$, but no trends with σ_g. At $z \simeq 3$, nearly all galaxies are small, but have large rotation velocities.

9. CONCLUSIONS

We use a sample of 544 galaxies to study the internal kinematics of blue galaxies over the last ~ 8 billion years, and find significant evolution. Galaxies become progressively more well-ordered with time as disturbed motions decrease and rotation velocities increase. In addition, galaxy potential well depths increase with time. At all redshifts, the more massive galaxies are on average the most kinematically evolved. The lowest mass galaxies in our survey, which are observed at low redshift, are not well-ordered. They may be settling today, or may never become settled disks. These trends with mass are consistent with downsizing trends for other galaxy properties, and we refer to this phenomenon as "kinematic downsizing."

We define a kinematically settled disk galaxy as having a ratio of ordered to disordered motions (V_{rot}/σ_g) of 3. We find that the fraction of settled disk galaxies, f_{settle}, increases with time since $z = 1.2$ for all but the lowest mass bin in our survey, which we can only probe at low redshifts. The fraction f_{settle} is larger the more massive the galaxy population is, and this is independent of redshift. These results do not change qualitatively if a settled disk galaxy is defined with values of V_{rot}/σ_g between 1 and 5.

We speculate that this evolution may be due to a decreasing rate of minor mergers/mass accretion which is expected in a ΛCDM Universe (e.g., as invoked by Oser et al. 2012, to explain the evolution of early-type galaxies) and may be linked to the precipitous decrease in galaxy star-formation rate and molecular gas fraction since $z = 1.2$. Phenomena which are the causes and effects of star-formation, such as minor mergers/accretion and gas motions, may increase disturbed motions. In addition, the large molecular gas reservoirs of higher redshift galaxies (Daddi et al. 2010; Tacconi et al. 2010) provide fuel not only for for star-formation, but also for disturbed motions through the Toomre Q parameter (Toomre 1964) as in e.g., Silk & Norman (2009). In addition, kinematic downsizing may be an effect of star-formation which began earlier and declined more quickly in massive galaxies, compared with a later on-set of star-formation in less massive systems. And this might be related to the minor merger rates for high and low mass galaxies.

We compile measurements of galaxy kinematics from the literature over $0 < z < 3.8$. Observations of the kinematics of local disk galaxies reveal few examples of massive disk galaxies where disturbed motions play as an important of a role as in similar mass disk galaxies at higher redshifts (e.g., Epinat et al. 2010). Our compilation of measurements over $1.5 < z < 3.8$ shows no trends with redshift, likely due to sample selection, since only the most highly star-forming systems at these red-

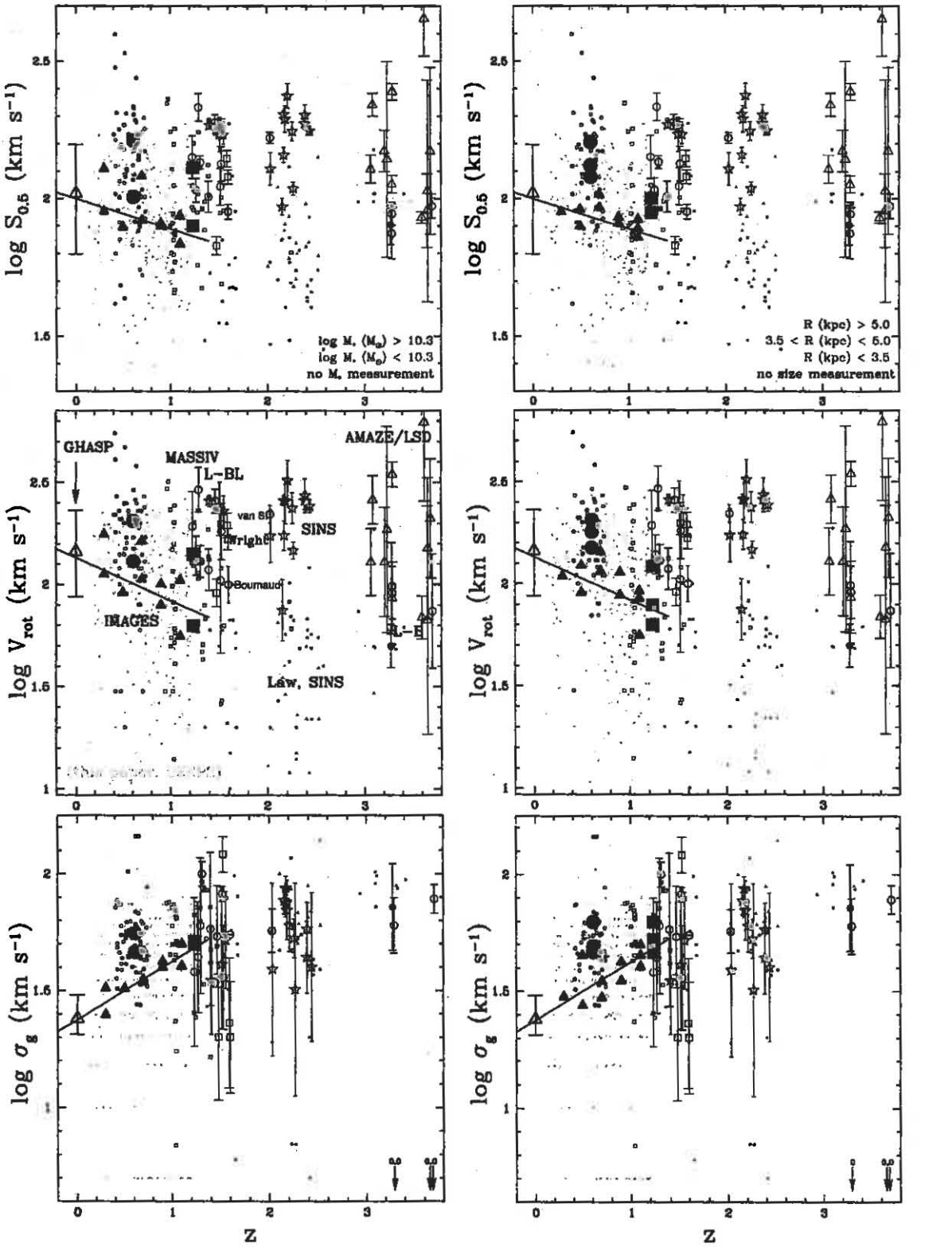

FIG. 12.— These plots are the same as in Figure 5, except here the z axes are expanded to include data from the literature for lower and higher redshift galaxies. In the plots on the left and right, galaxies are color-coded according to M_* and emission line extent, respectively. For galaxies the local GHASP survey, only the medians are shown (open black triangles), with error bars depicting the rms scatter. Otherwise, large open symbols denote individual galaxies where disk models were fit. Small filled points denote individual galaxies which were unable to be fit by a rotating disk model; for these galaxies, V_{shear} and an average σ_g are plotted. Large filled symbols represent survey medians. The providence of each galaxy from the literature is indicated by the symbol shape (regardless of whether it is open or filled), and references are labeled in the central panel on the left.

shifts can currently be studied. However, it is clear that most of these higher redshift systems have a significant amount of disturbed motions, whether or not they show evidence of rotation.

The exact causes of the disordered motions (as quantified by σ_g) are not yet known. They may indicate a formation mechanism for the thick disk, or a gas disk that is thickened by stirring, gas motions due to star-formation, and/or minor mergers. *Perhaps we are witnessing the phenomenon of disk settling as disturbed motions are turned into ordered rotation via mechanisms such as circularization of gas orbits and/or gaseous dissipation to the disk plane.* We do not yet know how this process of settling to a disk occurs, and whether baryonic dissipation is more similar to a smooth process or a repeated minor merging of clumps. Only with very high spatial resolution kinematic measurements, as can be obtained with IFS and adaptive optics on future 30–40-meter telescopes or the James Webb Space Telescope, will we be able to unambiguously reveal the nature of the processes which cause σ_g.

S.A.K is supported by an appointment to the NASA Postdoctoral Program at NASA's Goddard Space Flight Center, administered by Oak Ridge Associated Universities through a contract with NASA. The authors also acknowledge NSF grants AST 95-29098 and 00-71198 to UC Santa Cruz. S. A. K. kindly thanks F. Bournaud, N. Förster-Schreiber, A. Gnerucci, M. Puech, P. van der Werf, and S. Wright for providing tables of measurements and/or further information on how their measurements were performed.

REFERENCES

Abraham, R. G. et al. 1996, ApJS, 107, 1
Abraham, R. G. & van den Bergh, S. 2001, Science, 293, 1273
Bell, E. F. et al. 2005, ApJ, 625, 23
Binney, J. & Tremaine, S. 1987, Galactic Dynamics (Princeton: Princeton Univ. Press)
Blumenthal. G. R., Faber, S. M., Primack, J. R., & Rees, M. J. 1984, Nature, 311, 517
Borch, A. et al. 2006, A&A, 453, 869
Bournaud, F. et al. 2008, A&A, 486, 741
Bruzual, G. & Charlot, S. 2003, MNRAS, 344, 1000
Bundy, K. et al. 2006, ApJ, 651, 120
Catinella, B. 2012, MNRAS, 420, 1959
Chabrier, G. 2003, PASP, 115, 763
Contini, T. et al. 2012, A&A, 539, 91
Covington, M. et al. 2010, ApJ, 710, 279
Cowie, L. L. et al. 1996, AJ, 112, 839
Cresci, G. et al. 2009, ApJ, 697, 115
Daddi, E. et al. 2010, ApJ, 713, 686
Danovich, M., Dekel, A., Hahn, O., & Teyssier, R. 2011, arXiv:1110.6209
Davies, R. et al. 2011, ApJ, 741, 69
Dekel, A. & Birnboim, Y. 2006, MNRAS, 368, 2
Drory, N. 2009, ApJ, 707, 1595
Dutton, A. A. et al. 2011, MNRAS, 410, 1660
Epinat, B. et al. 2008, MNRAS, 388, 500
Epinat, B. et al. 2009, A&A, 504, 789
Epinat, B. et al. 2010, MNRAS, 401, 2113
Erb, D. K. et al. 2004, ApJ, 612, 122
Erb, D. K. et al. 2006, ApJ, 646, 107
Faber, S. M. 2003, SPIE, 4841, 1657
Faber, S. M. 2007, ApJ, 665, 265
Fall, S. M. & Efstathiou, G. 1980, MNRAS, 193, 189
Förster-Schreiber, N. M. 2009, ApJ, 706, 1364
Garrido, O. et al. 2005, MNRAS, 127, 166
Genzel, R. et al. 2008, ApJ, 687, 59
Gnerucci, A. et al. 2011, A&A, 528, 88
Kassin, S. A. et al. 2007, ApJL, 660, 35
Kassin, S. A. et al. 2011, MNRAS, 417, 2882
Kimm, T. et al. 2011, arXiv:1106.0538
Law, D. R. et al. 2009, ApJ, 697, 2057
Lemoine-Busserolle, M. et al. 2010, MNRAS, 401, 1657
Lemoine-Busserolle, M. & Lamareille, F. 2010, MNRAS, 402, 2291
Lotz, J. M. et al. 2011, ApJ, 742, 103
Madau, P., Pozzetti, L., & Dickinson, M. 1998, ApJ, 498, 106
Miller, S. H. et al. 2011, ApJ, 741, 115
Miller, S. H. et al. 2012, arXiv:1201.4386
Neichel, B. et al. 2008, A&A, 484 159
Newman, J. A. et al. 2012, ApJ submitted, arXiv:1203.3192
Noeske, K. G. et al. 2007, ApJL, 660, 43
Noeske, K. G. et al. 2007, ApJL, 660, 47
Oser, L. et al. 2012, ApJ, 744, 63
Pozzetti, L. et al. 2010, A&A, 523, 13
Puech, M. et al. 2007, A&A, 466, 83
Puech, M. et al. 2008, A&A, 173, 187
Puech, M. et al. 2010, A&A, 510, 68
Rees, M. J. & Ostriker, J. P. 1977, MNRAS, 179, 541
Silk, J. & Norman, C. 2009, ApJ, 700, 262
Sinard, L. et al. 2002, ApJS, 142, 1
Tacconi, L. J. et al. 2010, Nature, 463, 781
Toomre, A. 1964, ApJ, 139, 1217
van Starkenburg , L. et al. 2008, A&A, 488, 99
Vergani, D. et al. 2012, A&A accepted, arXiv:1202.3107
Weiner, B. J. et al. 2006, ApJ, 653, 1027
Weiner, B. J. et al. 2006, ApJ, 653, 1049
White, S. D. M. & Rees, M. J. 1978, MNRAS, 183, 341
White, S. D. M. & Frenk, C. S. 1991, ApJ, 379, 52
White S. D. M., 1996, in Schaefer R., Silk J., Spiro M., Zinn-Justin J., eds, Cosmology and Large-Scale Structure. Elsevier, Dordrecht, astro-ph/9410043
Willmer, C. N. A. et al. 2006, ApJ, 647, 853
Wirth, G. D. et al. 2004, AJ, 127, 3121
Wright, S. et al. 2007, ApJ, 658, 78
Wright, S. et al. 2009, ApJ, 699, 421
Yang, Y. et al. 2008, A&A, 477, 789